Tunable Emission in Aggregated T-Shaped 2*H*-Benzo[*d*][1,2,3]triazoles with Waveguide Behaviour

I. Torres,[a] A. Díaz-Ortiz,[a] L. Sánchez,[b] J. Orduna,[c] M. J. Blesa,[c] J. R. Carrillo,[*a] and P. Prieto [*a]

a Departamento de Química Orgánica, Facultad de Ciencias y Tecnologías Químicas, Universidad de Castilla-La Mancha, 13071-Ciudad Real, Spain.

b Departamento de Química Orgánica, Facultad de Ciencias Químicas, Universidad Complutense de Madrid, 28040-Madrid, Spain.

c Departamento de Química Orgánica, Facultad de Ciencias-Instituto de Ciencias de los Materiales de Aragón, Universidad de Zaragoza-CSIC, 50009-Zaragoza, Spain.

ABSTRACT

Symmetrical Donor-Acceptor-Donor (D-A-D) 2*H*-benzo[*d*][1,2,3]triazole derivatives have been designed by DFT calculations and prepared by a multistep synthetic protocol. The design strategy involved the identification of a suitable acceptor benzotriazole core and modification of the steric volume and donor strength of the branches in order to modulate the Intramolecular Charge Transfer (ICT) process and, consequently, the band gap. Self-assembly of the reported triazoles afforded organized supramolecular structures, the morphologies of which were visualized by SEM imaging. The outcomes demonstrated the effect that the donor moiety has on the emission properties and the morphologies of the aggregates. The aggregates that had a crystal-like structure, with smooth surfaces and flat end facets, exhibited optical waveguide behaviour with tunable colour emission. Depending on the initial design, the different emission wavelengths are related to the band gap of the benzotriazole derivatives.

Keywords

Tunable colour emission

Waveguide

* Corresponding author
E-mail address: mariapilar.prieto@uclm.es (P. Prieto) joseramon.carrillo@uclm.es (J. R. Carrillo)

Self-Assembly

T-shaped 2*H*-benzo[*d*][1,2,3]triazole

1. Introduction

Organic molecules that exhibit intense and tunable emission have received a great deal of attention and play an important role in next-generation of electronic applications due to their processability, flexibility, ultrathin aspect and large area. Among these organic nanomaterials, one-dimensional (1D) nanostructures have proven to be effective building blocks for miniaturized devices. In this respect, it is worth highlighting tunable color displays, like Organic Light-Emitting Diodes (OLEDs) [1], Organic Field-Effect Transistors (OFETs) [2], chemical sensors [3] and optical and optoelectronic devices such as lasers [4] and optical waveguides [5].

1D organic nano- and micro- structures have emerged as effective flexible media to generate or propagate and manipulate light efficiently on the sub-wavelength scale and these are considered to be fundamental elements and interconnectors in optical circuits. Within this framework, organic molecular crystals can serve as active optical waveguides [6,7] since higher crystallinity improves the photon-crystal lattice interactions and the charge-transport mobility. A number of articles have been published to date regarding the use of organic compounds as optical waveguides. In many cases these compounds emit light from 400 to 600 nm. However, examples of organic waveguide materials with a red emission above 600 nm are still rare. [8]

The modification or alteration of chemical structures is a common approach to tune the solid-state luminescence properties of organic materials. Most 1D organic waveguides are fabricated from small molecules with a π-conjugated structure due to their capacity to delocalize (move) electrons. [9] This property, along with the ready availability, facile synthesis and high purity, makes these compounds attractive components for device applications.

The absorption in these π-conjugated systems can be modulated by the construction of low band gap organic materials in which electron donor (D) and electron acceptor (A) moieties are incorporated into the molecular building blocks. This design facilitates intramolecular charge transfer (ICT). [10] As a consequence, the band gap levels and other related optical properties can

be readily tuned through the modification of donors and acceptors. Compared to the conventional D-A systems, other donor-acceptor-donor (D-A-D) types of chromophore will facilitate stronger ICT and lower the band gap energy further. [11] Moreover, the modification of moieties and substituents in conjugated structures not only provides strong ICT but also modulates the self-assembly behavior, facilitates crystal packing and contributes to their luminescence or the chromogenic phenomenon.

The introduction of heterocycles or heteroatoms into π-conjugated systems is also a useful approach for the construction of ICT compounds. [12] In this regard, benzotriazole is a moderate electron acceptor moiety for which it is assumed that the polarizable imine unit is responsible for its electronic character. [13] The introduction of different substituents on the nitrogen in the 2-position offers the possibility of modulating the electron acceptor properties. [14]

We are actively working on the synthesis of 4*H*-1,2,4-triazole and 2*H*-benzo[*d*][1,2,3]triazole derivatives that form aggregates which are capable of acting as tunable optical waveguides. [15-17] The latter series has a T-shaped geometry with spatial overlap between the HOMO and the LUMO, which is necessary for the large transition dipole moments that give rise to intense absorptions.

In this context, and as part of our ongoing research, we describe here the synthesis of T-shaped 2*H*-benzo[*d*][1,2,3]triazole D-A-D derivatives, the design of which was based on a computational study aimed at modulating the photoluminescent properties and self-assembly behaviour based on the peripheral donor groups. The properties of these aggregates as organic waveguides with tunable colour emission were studied.

2. Results and Discussion

Our initial goal was to develop a new series of T-shaped D-π-A-π-D benzotriazole derivatives with ICT character. The target compounds contain two electron-donor arms with different features and the benzotriazole unit as the electron-acceptor core. This design allows the efficient tuning of the HOMO-LUMO gap by changing the donor and acceptor groups. [18]

Structural modifications in molecular aggregates have a marked influence on their fluorescence properties such as the emission wavelength. [19] For this reason, a variety of aromatic moieties have been incorporated at the periphery of the D-A-D triad in order to modulate the aggregation process. This strategy provides an insight into structures-property relationships and this in turn enables the design of future derivatives.

2.1. Theoretical Approach

A very important aspect for the synthesis of compounds today is to implement a rational design strategy in order to obtain useful products and avoid the synthesis of unnecessary molecules – an approach that contributes to the sustainable development of chemistry. In this respect, Computational Chemistry is a useful tool to achieve this goal. [20]

With the above aim in mind, we initially performed computational calculations in order to gain an in-depth insight into the molecular geometries and the molecular orbital profiles of these compounds and to determine the photophysical and electrochemical properties. The theoretical outcomes were compared with the experimental results in order to direct future syntheses.

In an effort to modulate the emission properties, we first inserted different electron-withdrawing 2-arylsubstituents such as trifluoromethyl (**1a**), cyano (**1b**) and nitro (**1c**) in the 2-aryl-benzotriazole moiety (Figure 1). The decoration of the D-A-D triads with these acceptor moieties should decrease the LUMO energy of the designed materials, thus facilitating charge separation at the donor-acceptor heterojunction. The frontier molecular orbital profiles are shown in Figure 1.

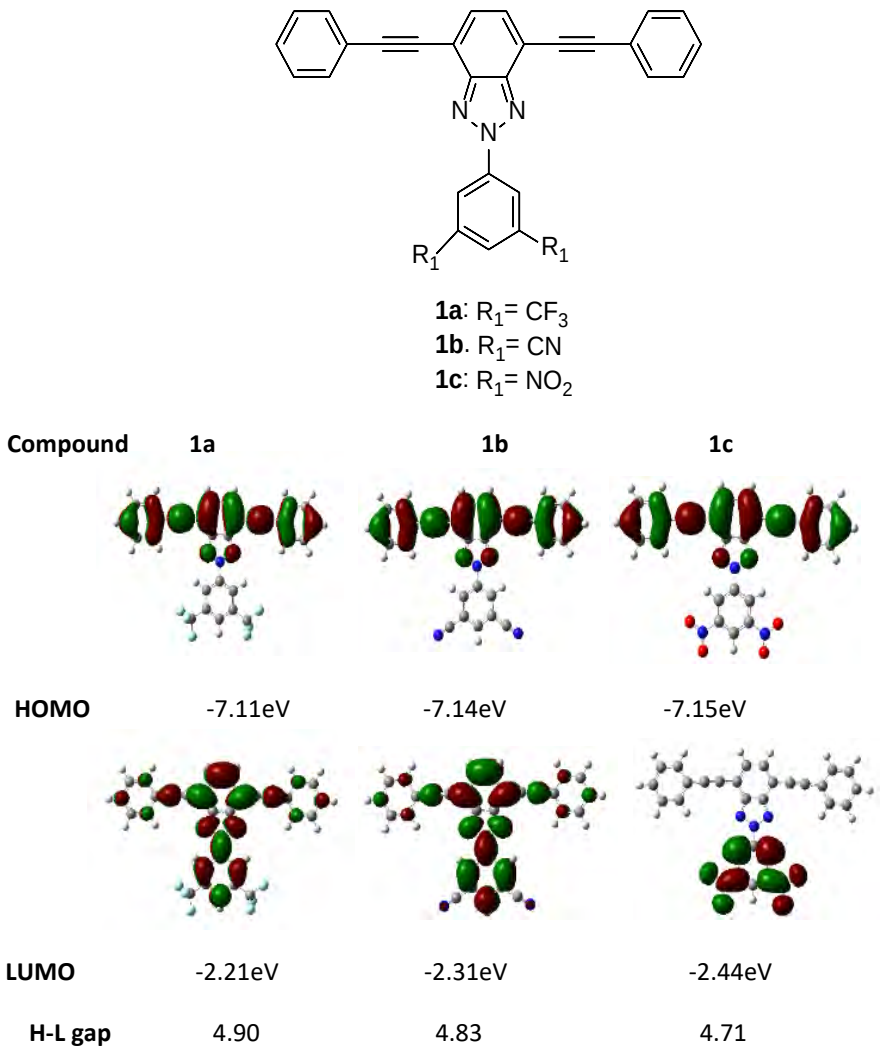

Figure 1. Topologies of the frontier molecular orbitals computed at CPCM-M06-2x/6-311+G(2d,p)//CPCM-M06-2x/6-31G*for compounds **1a**–**c**.

The introduction of two nitro groups (**1c**) decreases the band gap due to LUMO stabilization (Figure 1) but in this compound the LUMO is anchored on the nitro groups, thus preventing the necessary overlap of the frontier orbitals for the molecules to undergo a charge transfer process. In contrast, the introduction of trifluoromethyl or cyano groups (**1a** and **1b**, respectively) allows spatial overlap between the HOMO and the LUMO, which is necessary to achieve the large transition dipole moments that give rise to intense absorptions. In both cases, the band gap values were not modified substantially. Several examples have been reported in the literature of devices bearing trifluoromethylphenyl groups [21]. These compounds exhibit excellent electron-accepting properties and show a unique stacking tendency attributed to specific intermolecular interactions (C-F···H-C and C-F··· π). [22] Moreover, the densely packed fluorinated substituents

hinder the access of water and oxygen and also provide kinetic barriers to improve the ambient stability. For these reasons, [2-(3,5-bis(trifluoromethyl)phenyl]-4,7-bis(phenylethynyl)-2*H*-benzo[*d*][1,2,3]triazole (**1a**) was selected as the acceptor core.

We also selected several donor moieties with different characteristics to be attached to the acceptor unit (Compounds **1d**–**m**) (Figure 2). Aromatic moieties with different geometries were introduced: i.e., planar (**1d**–**j**) in order to favor aggregation by π-π stacking or twisted and bulky groups (**1k**–**m**) to decrease the π-π interactions in an effort to avoid low fluorescence quantum efficiency, which is mainly caused by π-π stacking of the planar backbones. [22] These structural modifications allowed the study of different aspects that could play an important role in the aggregation.

In the optimized structure the central 2-phenyl-4,7-bis(phenylethynyl)-2*H*-benzo[*d*][1,2,3]triazole unit is planar, with dihedral angles close to 0° (Figure 3a).

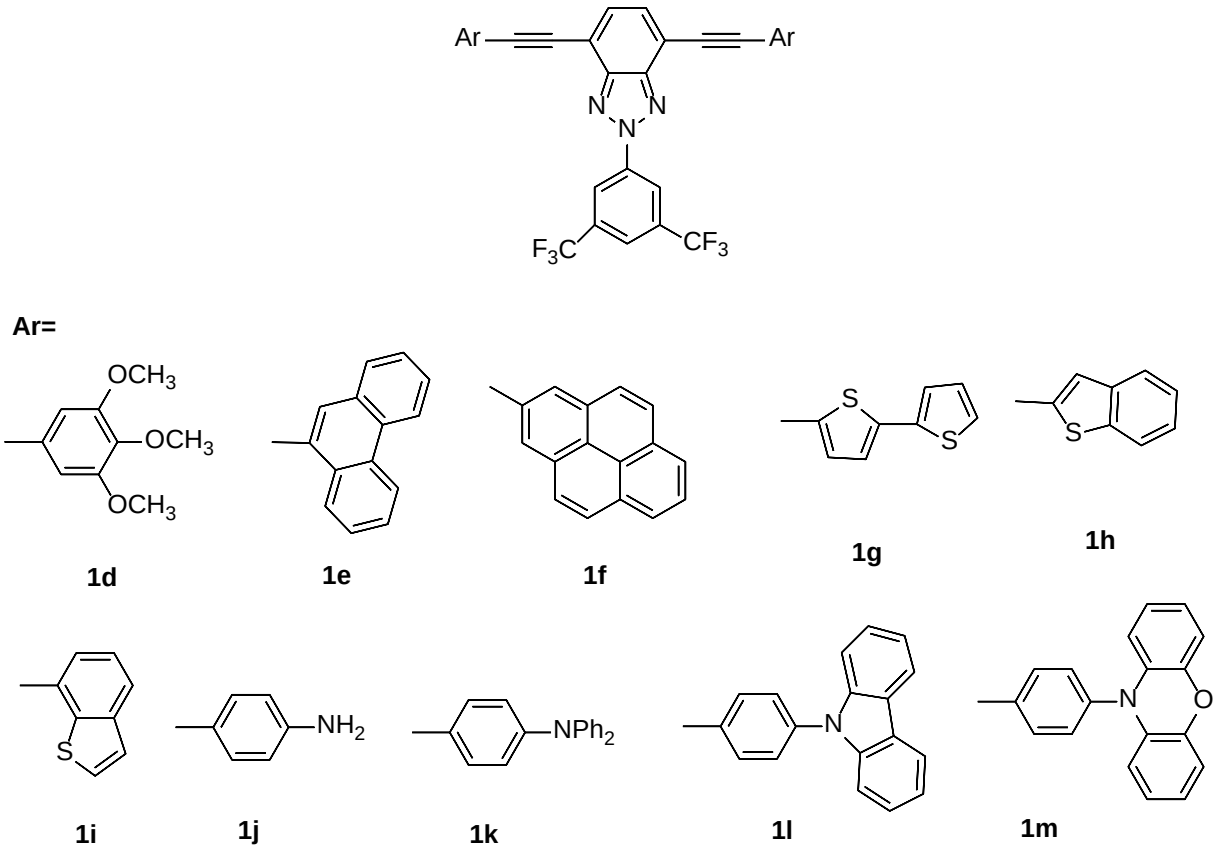

Figure 2. Set of designed ICT compounds (**1d**–**m**).

As expected, compounds **1d**–**j** have a planar arrangement (Figure 3a) whereas chromophores **1k**–**m** have a dihedral angle that deviates by 105–130° from planarity due to the increased steric hindrance between the benzotriazole ring and the arylalkynyl substituent (Figure 3b).

It is worth noting that in those cases in which there are two possible conformations, the most stable one is that in which the Ar group is closer to the nitrogen atoms of the triazole ring, since this structure is favoured by the formation of hydrogen bonds (Compounds **1e**, **1f** and **1i**) (Figure 3c). It can be seen in Figure 3c that the most stable conformers of compounds **1e** and **1f** are stabilized by the formation of two H-bonds between N1 and an aromatic proton (2.5 Å) and by two H–F interactions (2.7 Å). Compound **1i** is stabilized by two H-bonds between the S atom and the *ortho*-proton of the 2N-aryl group (2.8 Å) and another two between the 2*H*-thienyl and a fluoro-substituent (2.7 Å). This situation leads to a subtle curvature of the triple bond. Furthermore, in compound **1f** a rotation of the N-aryl group occurs in order to form the H-bonds. In all cases, the frontier molecular orbital profiles show an overlap between the HOMO and LUMO on the central acceptor core, which facilitates charge transfer from the electron-donating and electron-withdrawing units (Figure 4 and Table S1). The calculated HOMO-LUMO energies are collected in Table 1.

a) Front and side views of compound **1j**

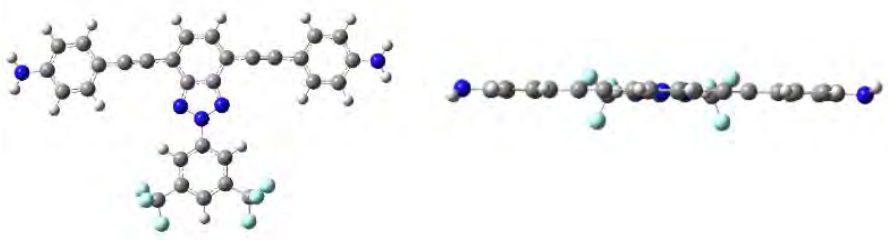

b) Front view of compound **1m**

c) Optimized structures of compounds **1e**, **1f** and **1i**

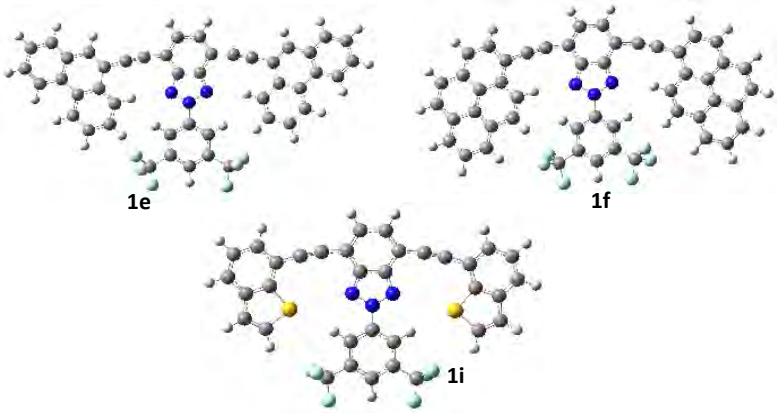

Figure 3. Optimized structures at M062x/6-31G* of different 2*H*-benzo[d][1,2,3]triazole derivatives.

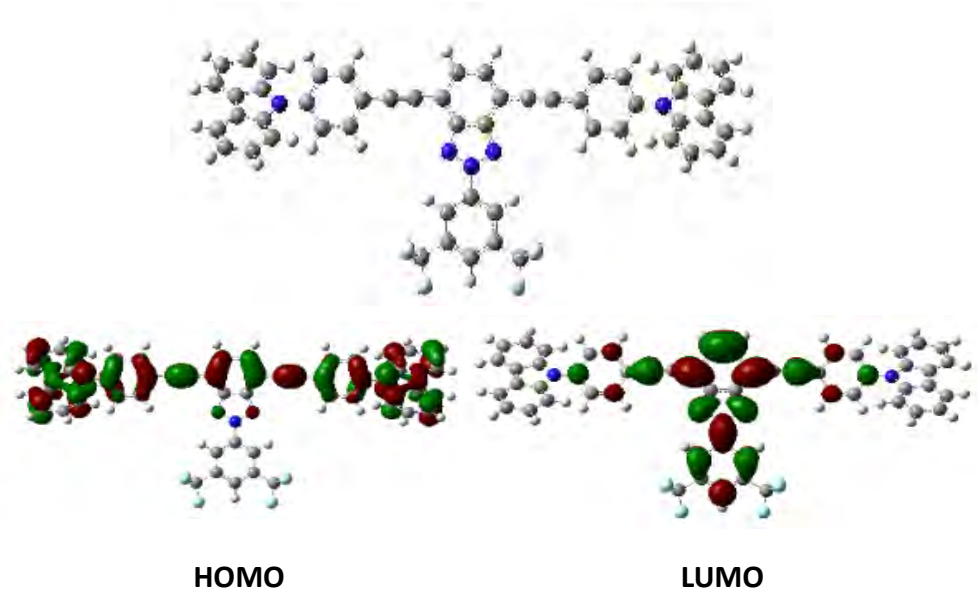

Figure 4. Topology of molecular orbitals computed at CPCM-M06-2x/6-311+G(2d,p)//CPCM-M06-2x/6-31G* for compound **1l**.

Table 1. Energy values (eV) of frontier molecular orbitals and HOMO-LUMO gaps for all compounds computed at the CPCM-M06-2x/6-311+G(2d,p)//CPCM-M06-2x/6-31G* theory level.

Compound	E_{HOMO} (eV)	E_{LUMO} (eV)	HOMO-LUMO gap (eV)
1a	**–7.11**	**–2.21**	**4.90**
1b	**–7.14**	**–2.31**	**4.83**
1c	**–7.15**	**–2.44**	**4.73**
1d	**–7.00**	**–2.19**	**4.71**
1e	**–6.64**	**–2.00**	**4.64**
1f	**–6.72**	**–2.32**	**4.40**
1g	**–6.64**	**–2.32**	**4.32**
1h	**–6.44**	**–2.31**	**4.13**
1i	**–6.98**	**–2.27**	**4.71**
1j	**–6.52**	**–2.06**	**4.46**
1k	**–6.38**	**–2.29**	**4.09**
1l	**–6.82**	**–2.28**	**4.54**
1m	**–6.52**	**–2.32**	**4.20**

These outcomes indicate that the HOMO-LUMO gap can be modulated by introducing different electron-donating groups. The lowest gaps correspond to substituents that bear a nitrogen with an available electron pair (compounds **1j**, **1k** and **1m**; Table 1) or thiophene derivatives (compounds **1g**, **1h**; Table 1) due to the more effective π-conjugation. The HOMO-LUMO gap values for

compounds **1h** and **1i** are markedly different despite the structural similarity (Table 1). Thus, compound **1h** has more effective π-conjugation and this results in stronger intramolecular interactions and a lower band gap.

2.2. Synthetic Procedure

Benzotriazoles **2** were prepared by the synthetic approach described by Höger from 1-nitro-2-nitrosobenzene and 3,5-bis(trifluoromethyl)aniline. [14] Bromination of **2** afforded the dibromobenzotriazole **3** in good yield (Scheme 1). A double Sonogashira C–C cross-coupling reaction between dibromobenzotriazole **3** and arylacetylenes **4** using reusable Pd-EnCat TPP30, 1,5-diazabicyclo[5.4.0]undecene-5-ene (DBU), CuI and MW irradiation as the energy source afforded arylalkynylbenzotriazoles **1** within 20 minutes in good to excellent yields. We recently employed this sustainable procedure for the preparation of triazole and benzotriazole derivatives. [17] All compounds gave satisfactory spectroscopic and analytical data.

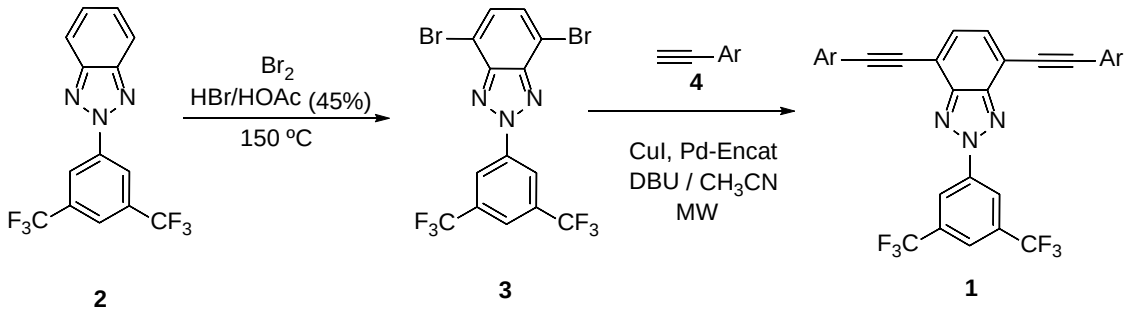

1d (3,4,5-trimetoxyphenyl) (83%); **1e** (phenantren) (80%); **1f** (pyren) (79%); **1g** (2,2´-bithiophen) (75%); **1h** (benzo[b]thiophen-2) (96%); **1i** (benzo[b]thiophen-7) (80%); **1j** (Aniline) (49%); **1k** (N,N-diphenyaniline) (90%); **1l** (9H-carbazole) (74%); **1m** (10H-pheoxacine) (82%).

Scheme 1. Synthesis of 2-(3,5-bis(trifluoromethyl)phenyl)-4,7-bis(phenylethynyl)-2*H*-benzo[*d*][1,2,3]triazole derivatives (**1**) by a Sonogashira cross-coupling between **3** and **4**.

2.3. Photophysical Properties

The electronic spectra of compounds **1d**–**m** were theoretically calculated and experimentally measured. The theoretical spectra were calculated in chloroform solution using the conductor-like polarizable continuum model (CPCM) [23] and the time-dependent density functional theory (TD-DFT) approach. [24] The M06-2X [25] meta-exchange functional was employed. This functional was chosen based on the accurate results obtained in the calculation of systems with high spatial orbital overlap, which are even better than those provided by the more widely used CAM-B3LYP. [26]

The electronic absorption and photoluminescence (PL) spectra were experimentally measured in $CHCl_3$ solutions at a concentration of 10^{-5} M (Figures 5 and 6). The photoluminescence (PL) behaviour was explored by excitation of the molecules at their absorption maxima. The most meaningful photophysical data are summarized in Table 2.

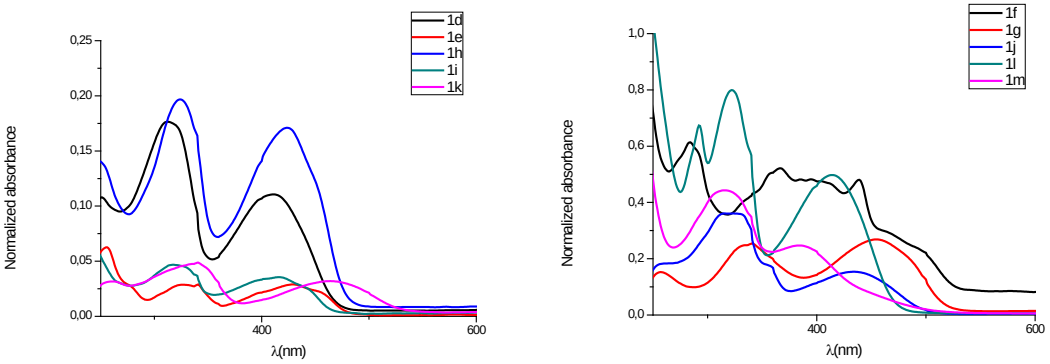

Figure 5. UV/Visible absorption spectra of compounds **1d**–**m** (298 K, $CHCl_3$, 1×10^{-5} M).

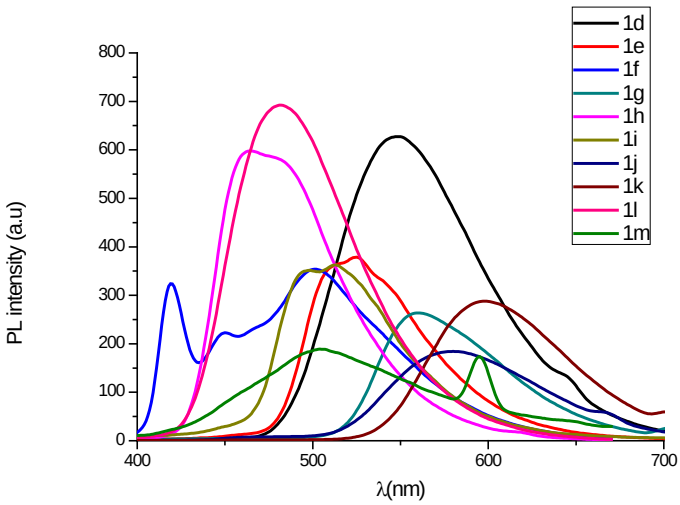

Figure 6. Emission spectra of compounds **1d**–**m** (298 K, $CHCl_3$, 1×10^{-5} M). All PL spectra were measured after excitation at the maximum absorption peak of the corresponding compounds.

Table 2. λ_{abs}, λ_{em} and Stokes shift (in nm) measured experimentally and calculated at the CPCM-M06-2x/6-311+G(2d,p)//CPCM-M06-2x/6-31G* theory level for compounds **1d**–**m**.

Comp.	λ_{abs} (nm) exp	λ_{abs} (nm) calc.	λ_{em} (nm) exp.	λ_{em} (nm) calc.	Stokes shift (nm)[a]	Φ [b]
1d	412	405	529	503	127 (98)	0.71
1e	421	426	529	530	108 (104)	0.61
1f	439	434	531	522	92 (88)	0.35
1g	455	460	562	587	107 (127)	0.17
1h	424	492	485	617	61 (125)	0.53
1i	411	414	514	513	103 (99)	0.78
1j	434	437	569	555	135 (118)	0.49
1k	464	453	572	562	108 (109)	0.32
1l	414	416	512	518	98 (102)	0.86
1m	384	398	510	522	126 (124)	0.32

(a) Calculated Stokes shift in brackets. (b) Φ is measured in $CHCl_3$ using Quinine Sulfate in H_2SO_4 1M (Φ=0.54) and 9,10-diphenylantracene in Ciclohexane (Φ=0.90)

With the exception of compound **1h**, the theoretical outcomes are in good agreement with the experimental results.

The UV-Visible spectra of all of the studied compounds have common features. For the sake of simplicity, these characteristis are explained on the basis of the calculations performed on **1d**.

The lowest energy and most intense absorption band at 412 nm, assigned to a one-electron HOMO-LUMO transition, was calculated at 405 nm to have an oscillator strength (*f*) of 1.64. The topology of these orbitals reveals that this transition involves a charge transfer from the aromatic rings at the horizontal extremes to the bis(trifluoromethyl)phenyl ring at the lowest end of the vertical axis (see Figure S1).

In contrast to the above, absorptions below 370 nm are the result of several overlapping transitions and, therefore, it is difficult to establish an unambiguous assignment. The calculations predict large absorption bands at 307 nm (f = 0.51) and 284 nm (f = 0.84) and a less intense absorption band at 290 nm (f = 0.28). Absorption at 307 nm is mainly due to a HOMO-4 to LUMO transition and therefore does not involve charge transfer since both molecular orbitals are localized on the vertical branch of the molecule. The absorptions at 290 and 284 nm involve HOMO-1 to LUMO and HOMO to LUMO+1 transitions, respectively. Both of these therefore have a charge-transfer character as electronic density is translated from the horizontal to the vertical branch of the molecule.

The spectra of molecules **1e**–**m** display a similar pattern but are further complicated due to the effect of substituents. The complete results are included in the supplementary information file.

All of the PL curves of the D-A-D chromophores contain only one resolved ICT emission band (Figure 6). Compound **1k** shows the longest absorption and emission peak and this is consistent with the bulky triphenylamine (TPA) skeleton, which makes efficient π-stacking difficult. In contrast, the flatter carbazolyl-containing **1l**, which has similar electronic features to TPA, shows a hypsochromic shift of 50 nm in the absorption spectrum and 60 nm in the emission spectrum in comparison to **1k**. Recently, it was reported that the high fluorescence of TPA is attributed not only to the bulky skeleton but also to the intercrossed excited state between the low-lying local exciton (LE) and charge transfer (CT) exciton resulting from the D-A structure. [27] This result

is consistent with the calculated band gap values, since **1k** has the lowest value of all the compounds reported here.

It is remarkable that the stronger electron-donating ability of the thiophene ring in comparison to the benzene ring gives rise to more effective π-conjugation, which in turn results in stronger intramolecular interactions and a lower band gap. Thus, compound **1g** shows a bathochromic shift in the spectrum in comparison to **1e**.

Large Stokes shifts of around 100 nm (Table 2) can be observed for all T-shaped chromophores and this finding is attributed to the ICT nature of the excited state. [28] Large Stokes shifts can improve the efficient waveguiding behaviour by avoiding the loss of light caused by self-absorption.

Compounds **1d**, **1e**, **1i** and **1l** are high emissive with a fluorescence quantum yields of 0.71, 0.61, 0.78 and 0.86, respectively

The prepared chromophores were further investigated by studying solvatochromic effects. Only compounds **1j**, **1k** and **1m** showed a solvatochromic effect (Figures 7 and S2, S3). The ICT absorption band of these compounds changed slightly on increasing the permittivity of the solvent. In contrast, the emission peak moved markedly on increasing the solvent polarity from cyclohexane to DMF (Figure **7c**–**d**). This effect is ascribed to a large dipole moment in the excited state when compared to that in the ground state. [29] Therefore, a more polar solvent is able to stabilize such a polarized excited state by reorientation of the solvent molecules to accommodate the increased dipole, thus lowering the energy of the system and thereby leading to a more distinct bathochromic shift in the PL spectra.

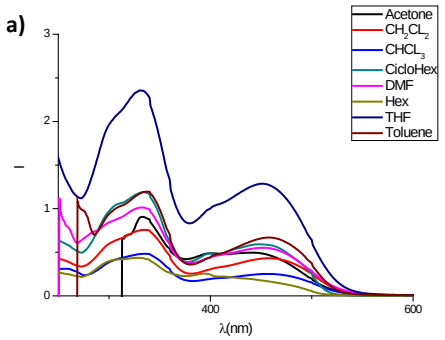

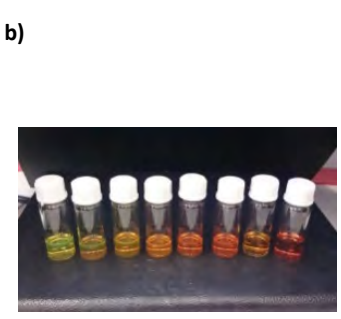

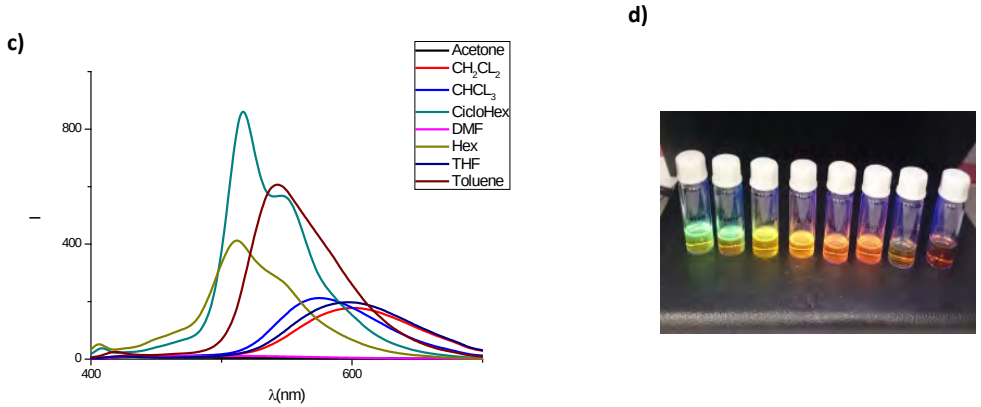

Figure 7. UV-Vis absorption (a) and fluorescence (c) spectra in different solvents with varying polarities for compound **1k**. The concentration of each sample was 10^{-5} M. Luminescence photographs of **1k** in hexane, cyclohexane, $CHCl_3$, toluene, dichloromethane, THF, acetone and dimethylformamide upon excitation at 254 nm (b) and 365 nm (d).

2.5. Electrochemical Properties

The redox properties of the reported T-shaped benzotriazoles derivatives were followed by Cyclic Voltammetry (CV) and Differential Pulse Voltammetry (DPV). The oxidation potential is determined by the anodic peak of the voltamogram (DPV). The redox potentials were also calculated theoretically (Table 3). It can be seen that there is reasonable agreement between the calculated and experimental values. Most of the compounds show two irreversible waves corresponding to both the oxidation of the donor and the reduction of the acceptor moieties (Figures S4-S13).

Compounds **1d**–**1m** have different donor moieties and their strength is mirrored by the decrease of E_{ox}. In contrast, the E_{red} does not show any noticeable variations.

Compounds **1j, 1k** and **1m** have substituents with one available electron pair on a nitrogen atom in their structure and these compounds show better donor properties than compound **1l** (without an available nitrogen lone pair) (Table 3, entries 7, 8, 10).

Moreover, the behaviour of compounds **1g**, **1h** and **1i** (with a thiophene moiety in the spacer) hinders, as one would expect, the oxidation and reduction processes. This behaviour can be related to the delocalisation of the positive and negative charges in the electrogenerated ion radicals. The delocalisation disrupts the aromaticity of the thiophene ring, thus leading to a higher energetic cost (Table 3, entries 4, 5, 6).

On passing from **1d** to **1j** there is a shift in the E_{ox} value towards a less anodic potential and this shows the superior donor ability of the nitrogen derivative **1j** compared to the oxygen derivative **1d**. This finding is in good agreement with the calculated trends for redox potentials (Table 3, entries 1, 7) and the corresponding E_{HOMO} and E_{LUMO} values (Table 1, entries 4,10).

Table 3. Electrochemical properties of compounds **1d**–**m**

Entry		**E_{ox}[a]**		**E_{red}[a]**	
		Calc[d.]	**exp[b]**	**Calc[d.]**	**exp[b]**
1	**1d**	1.63	1.38	–1.63	-1.12
2	**1e**	1.61	1.50	–1.54	-1.06
3	**1f**	1.40	1.48	–1.63	-1.15
4	**1g**	1.40	1.49	–1.52	-1.00
5	**1h**	1.16	1.58	–1.54	-1.06
6	**1i**	1.63	1.69	–1.49	-1.17
7	**1j**	1.07	0.87	–1.72	-1.05
8	**1k**	1.17	1.13[c]	–1.64	-1.13
9	**1l**	1.58	1.50	-1.48	-1.03
10	**1m**	1.44	0.85[c]	-1.51	-1.00

[a] versus Ag/AgCl. [b] 1-5 × 10^{-4} M in $CHCl_3$, glassy carbon working electrode, Pt counter electrode, 20 °C, 0.1 M NBu_4PF_6, 50 mV s^{-1} scan rate. Ferrocene internal reference $E_{1/2}$ = +0.51 V. [c] $E_{ox}=E_{1/2}$

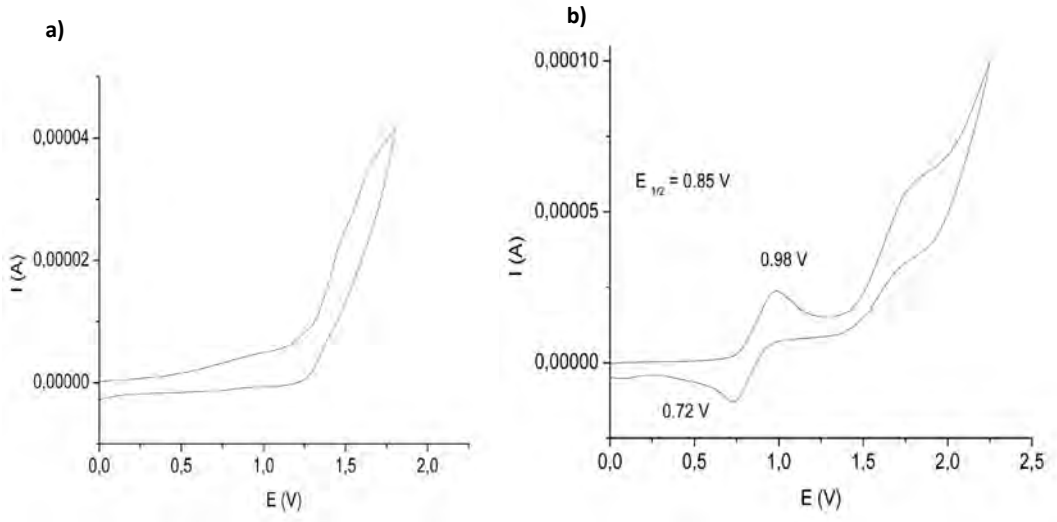

Figure 8. Cyclic Voltammograms of compounds **1d** (a) and **1m** (b).

Compounds **1d**–**1m** have different donor moieties and their strength is mirrored by the decrease in E_{ox}. In contrast, the E_{red} values do not vary significantly. Compounds **1j**, **1k** and **1m** bear substituents that contain a nitrogen atom and these show better donor properties than compound **1l** (without an available nitrogen lone pair) due to the presence of the electron pair on this heteroatom (Table 3, entries 7, 8, 10).

Moreover, the behaviour of compounds **1g**, **1h** and **1i** indicates that the presence of a thiophene moiety in the spacer hinders the oxidation and reduction processes. This behaviour can be related to the delocalization of the positive and negative charges in the electrogenerated radical ions. The delocalization disrupts the aromaticity of the thiophene ring, thus leading to a higher energetic cost (Table 3, entries 4, 5, 6).

On passing from **1d** to **1j** there is a shift in the E_{ox} value towards a less anodic potential and this shows the superior donor ability of the nitrogen derivative **1j** compared to the oxygen derivative **1d**. This finding is in good agreement with the calculated trends for redox potentials (Table 3) and the corresponding E_{HOMO} and E_{LUMO} values (Table 1) used to modulate HOMO-LUMO gaps.

2.6. Self-Assembly

The formation of organized structures is a crucial aspect in the applicability of organic materials in a variety of research areas such as organic photovoltaics, emitting diodes and even catalysis. [30] With this target in mind, and on the basis of the optoelectronic and electrochemical properties shown by the compounds described above, we focused our attention on the formation of supramolecular structures with potential applications in organic optoelectronic devices, particularly as optical waveguides.

When compared with the vapour phase deposition method, self-assembly in a liquid phase is a more facile and low-cost way to construct organic crystalline micro-/nanostructures. The slow diffusion technique was employed to achieve the supramolecular structures with benzotriazoles **1d**–**m**. Thus, a dilute solution (10^{-4} M) of these compounds in a good solvent, like $CHCl_3$ or THF, was gently placed in a vessel containing a poor solvent (MeOH, CH_3CN or hexane). After several days of slow diffusion, a precipitate was observed in the vial. $CHCl_3$/MeOH proved to be the best mixture of the six combinations evaluated. This mixture led to the formation of aggregates of all compounds except for **1d**. In our previous studies it was observed that MeOH induces the formation of well-defined morphologies. [15-17] The as-prepared aggregates were studied by scanning electron microscopy (SEM) on glass substrates. SEM images showed the formation of aggregates with different morphologies depending on the chemical structure of the peripheral substituent.

Compounds **1f** and **1k** showed a very low tendency to form organized aggregates and only amorphous precipitates were obtained (Figures S14 and S15). The low solubility of the pyrene derivative prevented the formation of aggregates (**1f**) and the bulky triphenylamine moiety (**1k**) makes efficient π-π interactions between the aromatic units difficult. Similar behaviour was found for the amino derivative **1j**, which aggregated as an amorphous solid but only when chloroform was used as the good solvent (Figure S16). In contrast, bisthienyl derivative **1g** formed organized aggregates in all solvent mixtures tested. The morphology of these aggregates depended on the solvent employed. In some cases, the precipitates showed ribbon-like structures aggregated

around a nucleation centre (Figure 9a) or flower-like structures when hexane was used as the poor solvent (Figure 9b).

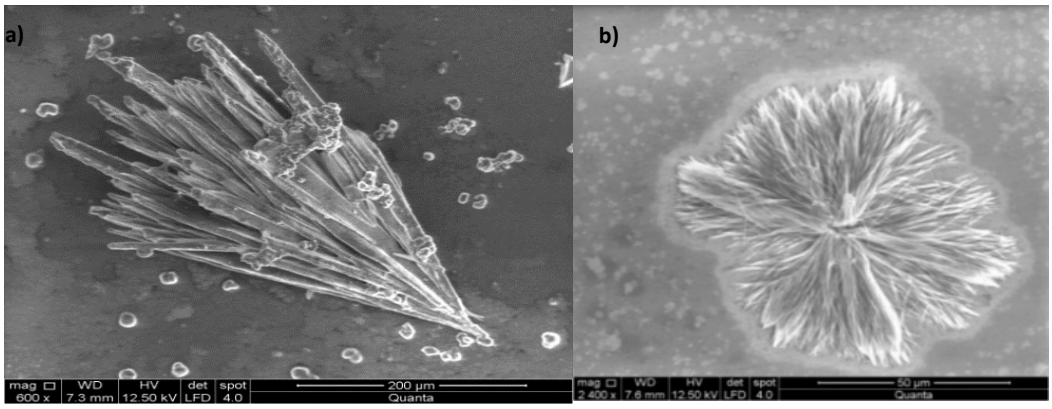

Figure 9. SEM images (glass substrate, 298 K) of the aggregates formed by **1g** (obtained by slow diffusion of THF/CH_3OH (a) and THF/Hexane (b)).

It was previously observed that the presence of methoxyl groups on the periphery played an important role in the formation of aggregates, since the methoxyl group induces non-covalent interactions by hydrogen bonds between neighbouring molecules. [16,17] Unexpectedly, the methoxy derivative **1d** showed a low tendency to form organized aggregates and lace-like structures were obtained on using chloroform or THF as the good solvent and methanol and hexane as the poor solvents (Figure 10).

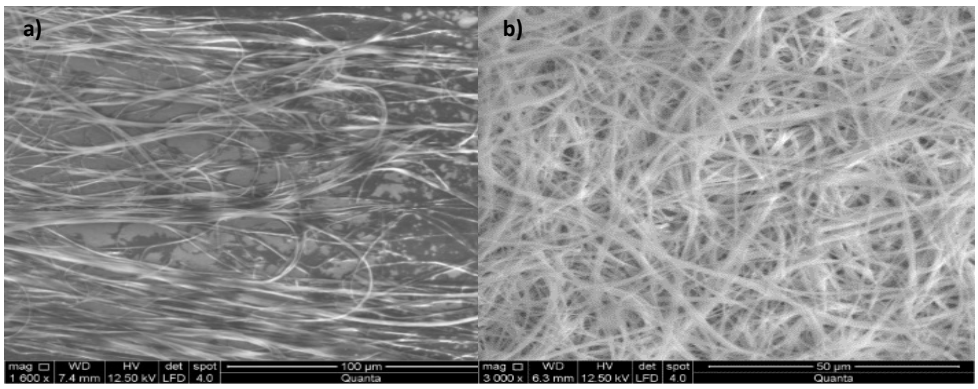

Figure 10. SEM images (glass substrate, 298 K) of the aggregates formed by **1d** (obtained by slow diffusion of THF/CH_3OH (a) and THF/Hexane (b)).

The aggregates obtained from the benzotriazole derivative with a phenoxazine as the peripherical group (**1m**) were organized into rod-like structures in $CHCl_3$/CH_3CN (Figure 11). The use of CH_3OH as the poor solvent in the slow diffusion process resulted in an amorphous material.

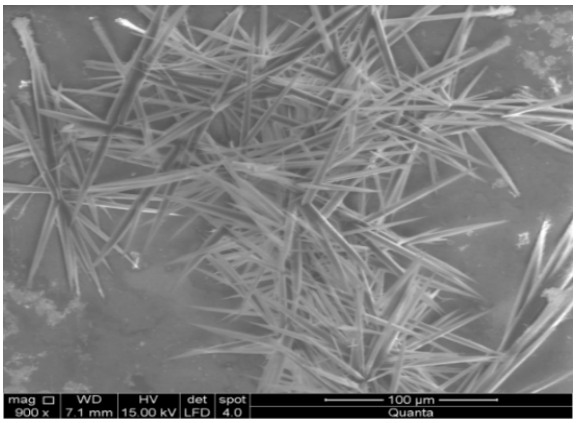

Figure 11. SEM images (glass substrate, 298 K) of the aggregates of **1m** (obtained by slow diffusion of $CHCl_3$/CH_3CN).

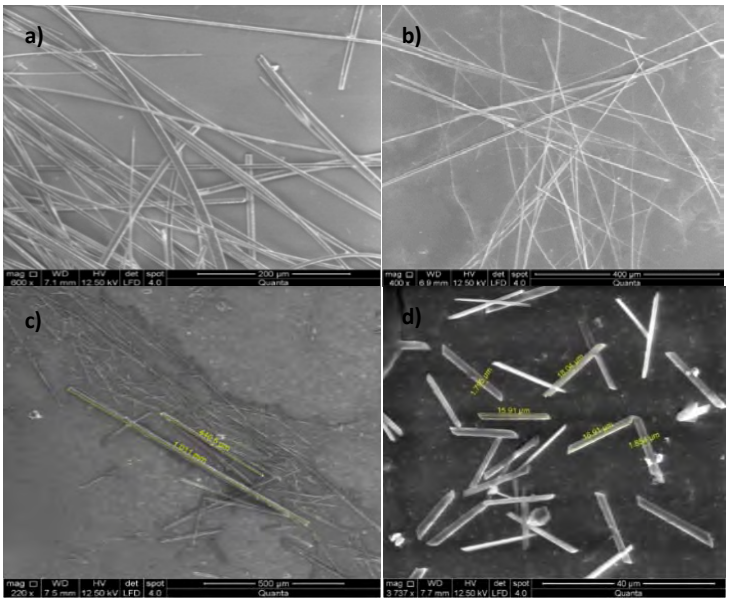

Figure 12. SEM images of the supramolecular structures formed by the self-assembly of benzotriazole derivatives **1e** (a); **1h** (b); **1i** (c) and **1l** (d). The samples in (a) and (b) were obtained by the slow diffusion technique on using $CHCl_3$ and Hexane as good and poor solvents,

respectively. The samples in (c) and (d) were prepared with THF/MeOH. All samples were prepared at a concentration of 10^{-4} M.

Finally, the self-assembly of compounds **1e**, **1h**, **1i** and **1l** using different solvent mixtures gave rise to thick and long crystalline needle-like structures (Figure 12) required for the desired waveguide behaviour. These rod-like aggregates have well-defined edges, probably due to the more efficient stacking of the aromatic moieties. It is worth noting that compound **1h** is the most prone to aggregation and it formed well-defined needles with a length of 700 μm and a width of 13 μm (Figure 12b).

2.7. Optical waveguide behaviour

Considering previous results on the optical waveguide features exhibited by triazoles [15-17] and in order to gain further insights into the light waveguide behaviour of organic micro/nanostructures, we investigated the propagation of light along the aggregates formed by the 2*H*-benzo[*d*][1,2,3]triazole derivatives discussed above.

Only aggregates that have a single-crystal structure, smooth surfaces and flat end facets can act as optical waveguides. For this reason, and on the basis of the SEM images, compounds **1d**, **1e**, **1h**, **1i**, **1l** and **1m** were selected for this study. The optical waveguide behaviour was evaluated using a fluorescence microscope. The abovementioned aggregates were irradiated with a light beam at different λ and the fluorescence was assessed.

The photoluminescence (PL) images of needle aggregates of compounds **1d**, **1e**, **1h**, **1i**, **1l** and **1m** are shown in Figure 13. All of these compounds exhibited bright luminescence spots at the two ends and a relatively weak emission from the bodies, which is characteristic of optical waveguides. This finding indicates the ability of these aggregates to absorb light and propagate PL towards the ends.

The waveguide behaviour of these aggregates can be explained by considering the separation between the emission and absorption bands mentioned above. This separation avoids re-

absorption of the emitted light by the aggregates. Furthermore, the well-defined smooth surface of the aggregates strongly contributes to the efficient propagation of light. It is well established that the presence of defects in the surface of the supramolecular structures produces light scattering due to internal reflections. [31]

As in our previous studies, compound **1d**, which has the highest band gap value, shows blue emission of light at both ends of the aggregates. Following this reasoning, in compounds with lower band gaps (**1e**, **1h**, **1i**, **1l**), green-red emission was detected at the ends of the thick filaments generated by self-assembly of these benzotriazole derivatives. The ability of these aggregates to emit at two wavelengths should be highlighted and this phenomenon is currently under investigation.

Finally, the aggregate of compound **1m**, which has the lowest band gap, only gave red emission and showed the longitudinal propagation of the light and highly brilliant spots that were visible at the opposite extremes of the aggregate.

The initial goal of our work was to model the band gap of benzotriazole derivatives in order to obtain aggregates that exhibit waveguide behaviour with different emission wavelengths and tuneable colours. The outcomes obtained show that this goal was achieved.

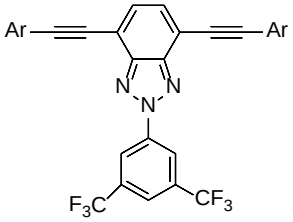

Ar-	Blue Waveguide	Green Waveguide	Red Waveguide
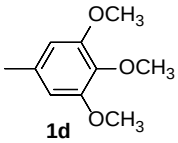 **1d**	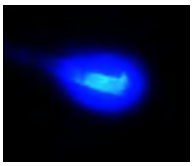		
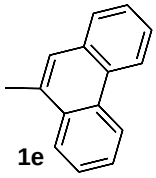 **1e**			
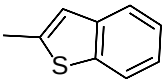 **1h**		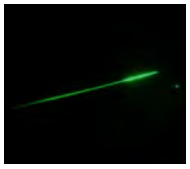	
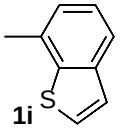 **1i**		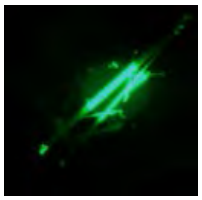	
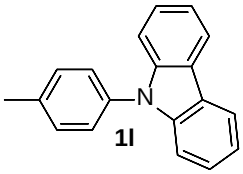 **1l**			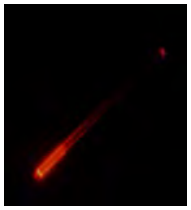
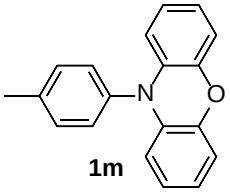 **1m**			

Figure 13. Fluorescence microscopy images of the aggregates of **1d**, **1e**, **1h**, **1i**, **1l** and **1m**.

3. Conclusions

T-shaped 2*H*-benzo[*d*][1,2,3]triazole derivatives with Internal Charge Transfer (ICT) behaviour have been studied by DFT/TD calculations. Several compounds were then synthesized using a sustainable methodology, i.e., microwave irradiation as the energy source, a marked decrease in the amount of solvent and the use of a reusable catalyst. The introduction of different donor substituents in the horizontal arm of these compounds allowed the HOMO-LUMO gap to be modulated in order to tune the emission properties.

The results obtained in the photophysical and electrochemical studies are consistent with the theoretical predictions and this validated the design strategy.

The aggregates generated from the self-assembly of the synthesised 2*H*-benzo[*d*][1,2,3]triazoles by the slow diffusion technique were studied by SEM imaging and the results demonstrate the enormous effect exerted by the peripheral substitution on the morphology of these aggregates.

According to our initial hypotheses, aggregates **1d**, **1e**, **1h**, **1i**, **1l** and **1m**, which have a tailored band gap, single-crystal structures, smooth surfaces and flat end facets, all show optical waveguide behaviour. A lower band gap led to a bathochromic displacement in the emission. In this sense, new compounds have been obtained that aggregate and can act as optical waveguides with tunable colour emissions between blue and red.

4. Experimental

4.1. General

Reagents were used as purchased. All air-sensitive reactions were carried out under an argon atmosphere. Flash chromatography was performed using silica gel (Merck, Kieselgel 60, 230–240 mesh or Scharlau 60, 230–240 mesh). Analytical thin layer chromatography (TLC) was performed using aluminium-coated Merck Kieselgel 60 F254 plates. NMR spectra were recorded on a Varian Unity 500 (^{1}H: 500 MHz; ^{13}C: 125 MHz) spectrometer at 298 K using deuterated solvents an internally referenced against the residual protio solvent signal. Coupling constants (J) are denoted in Hz and chemical shifts (δ) in ppm. Multiplicities are denoted as follows: s = singlet, d = doublet, t = triplet, m = multiplet, br = broad.

MALDI-TOF mass spectra were obtained on a Bruker Autoflex III TOF/TOF spectrometer (Bremen, Germany) operated in reflector mode and using dithranol as the matrix. Accurate mass measurements were performed using polyethylene glycol as internal standard and the spectra were calibrated using the $[HO(C_2H_4O)_nH + Na\ ]^+$ ions as reference masses. In a typical experiment, matrix (20 mg/mL), sample (1 mg/mL) and polyethylene glycol (10 mg/mL) were separately dissolved in methanol, mixed in a 5/1/1 ratio, deposited on the MALDI probe and air-dried.

SEM images were obtained on a JEOL JSM 6335F microscope working at 10 kV. The samples for SEM imaging were prepared by a controlled precipitation using the appropriate solvent or by slow diffusion by using mixtures of solvents, depending on their solubility properties (see the corresponding Figure Caption for a detailed description). The corresponding solid was deposited onto a glass substrate and the remaining solvent was slowly evaporated.

Electrochemical measurements were performed with a μ-Autolab ECO-Chemie potentiostat, using a glassy carbon working electrode, Pt counter electrode, and Ag/AgCl reference electrode. The experiments were carried out under argon, in $CHCl_3$, with Bu_4NPF_6 as supporting electrolyte (0.1 mol L^{-1}). The scan rate was 50 mV s^{-1} (Cyclic voltammetry) and 0.01 V s^{-1} (DPV). Modulation amplitude and modulation time were 0.025 V and 0.05 s^{-1} respectively.

UV-vis spectra were recorded on a Varian Cary model 5000 UV-Vis-NIR spectrophotometer, using standard quartz cells of 1 cm width and solvents of spectroscopic grade.

Fluorescence images were recorded on a Leica TCE SP2 confocal microscope with a mercury lamp capable of excitation at any wavelength. However, a series of filters was used to select the excitation wavelength and absorption. These correspond to wavelengths in the blue (λ_{exc} = 320–380 nm, λ_{em} = 410–510 nm), green (λ_{exc} = 4500–490 nm, λ_{em} = 515–565 nm) or red (λ_{exc} = 475–495 nm, λ_{em} = 520–570 nm).

Density functional theory (DFT) calculations were performed with the Gaussian 09 [32] suite of programmes using the M06-2X functional.[25] Solvent effects on molecular geometries and energies were estimated by means of polarization continuum models (CPCM) [23] using chloroform as solvent. Geometry optimizations were performed using the medium-sized 6-31G* basis set and frequency calculations were performed to confirm the nature of ground state

stationary points. Absorption spectra were calculated using single point time-dependent density functional theory (TD-DFT) [24] calculations and the large 6-311+G(2d,p) [33] basis set.

For the calculation of emission spectra, TD-DFDT calculations were performed at the optimized geometry of the first excited state using an identical model chemistry (M06-2x/6-311+G(2d,p)//M06-2x/6-31G*) and solvation model.

Ground state redox potentials were calculated from the difference in Gibbs free energy between neutral molecules and oxidized (or reduced) radical ions in solution using the CPCM solvation model [34]. The calculations of Gibbs free energies used M06-2x/6-311-G (2d,p) energies with thermal corrections calculated at the M06-2x/6-31G* level.

*4.2. Preparation of 2-(3,5-bis(trifluoromethyl)phenyl)-4,7-bis(arylethynyl)-2H-benzo[d][1,2,3] triazoles **1**.*

General procedure: A mixture of 2-(3,5-bis(trifluoromethyl)phenyl)-4,7-dibromo-2*H*benzo[*d*][1,2,3]triazole (**3**) (0.100 g, 0.2 mmol), the corresponding acetylene derivative (**4**) (0.4 mmol), DBU (0.061 g, 0.40 mmol), CuI (0.002 g, 0.01 mmol) and Pd-EncatTM TPP30 (0.018 g, 0.007 mmol) was charged under argon to a dried microwave vessel. CH_3CN (1 mL) was added. The vessel was closed and irradiated at 130 °C for 20 min. The crude reaction product was purified by chromatography, eluting with hexane/ethyl acetate to give analytically pure products **1**.

*4.2.1. 2-(3,5-bis(trifluoromethyl)phenyl)-4,7-bis((3,4,5-trimethoxyphenyl)ethynyl)-2H-benzo[d][1,2,3]triazole (**1d**)*: From 5-ethynyl-1,2,3-trimethoxybenzene (**4d**) (0.077 g, 0.40 mmol), derivative **1d** (0.114 g, 80%) was obtained as a yellow solid by chromatography eluting with hexane/ethyl acetate (5/1). M. p.: 172–174 °C. ^{1}H-NMR ($CDCl_3$, ppm) δ: 9.01 (s, 2H, *o*-N-Ph), 8.00 (s, 1H, *p*-N-Ph), 7.66 (s, 2H, H-benzotriazole), 6.94 (s, 4H, *o*-Ph), 3.93 (s, 12H, *m*-OCH_3), 3.91 (s, 6H, *p*-OCH_3). ^{13}C-NMR ($CDCl_3$, ppm) δ: 153.2, 145.5, 141.0, 139.6, 133.5, 131.8, 123.8, 122.6, 121.0, 117.6, 114.3, 109.2, 97.7, 84.0, 61.0, 56.2. MS calcd for ($C_{36}H_{27}F_6N_3O_6$) $M^{+\cdot}$ 711.1799, found 711.1830.

*4.2.2. 2-(3,5-bis(trifluoromethyl)phenyl)-4,7-bis(phenanthren-1-ylethynyl)-2H-benzo[d][1,2,3]triazole (**1e**)*: From 1-ethynylphenanthrene (**4e**) (0.081 g, 0.40 mmol), derivative **1e** (0.112 g, 77%) was obtained as a yellow solid by chromatography eluting with hexane/ethyl acetate (3/1). M. p.: 267–269 °C. ^{1}H-NMR ($CDCl_3$, ppm) δ: 9.13 (s, 2H, *o*-N-Ph), 8.91 (d, *J* = 7.8 Hz, 2H, H7-phenanthrene), 8.72 (d, *J* = 7.8 Hz, 2H, H6-phenanthrene), 8.26 (s, 1H H2-phenanthrene), 8.18 (d, *J* = 7.8 Hz, 2H, H3-phenanthrene), 8.16 (s, 1H, *p*-N-Ph), 7.95 (d, *J* = 7.8 Hz, 2H, H10-phenanthrene), 7.83 (s, 2H, H-benzotriazole), 7.83–7.77 (m, 4H, H5,H8-phenanthrene), 7.73 (t, *J* = 7.8 Hz, 2H, H4-phenanthrene), 7.65 (t, *J* = 7.8 Hz, 2H, H9-phenanthrene). MS calcd for ($C_{46}H_{23}F_6N_3$) $M^{+\cdot}$ 731.1791, found 731.1772.

*4.2.3. 2-(3,5-bis(trifluoromethyl)phenyl)-4,7-bis(pyren-1-ylethynyl)-2H-benzo[d][1,2,3]triazole (**1f**):* From 1-ethynylpyrene (**4f**) (0.090 g, 0.40 mmol), derivative **1f** (0.118 g, 76%) was obtained as a red solid by chromatography eluting with hexane/ethyl acetate (9/1). M. p.: 203–204 °C. MS calcd for ($C_{50}H_{23}F_6N_3$) $M^{+\cdot}$ 779.1791, found 779.1779.

*4.2.4. 4,7-bis((2,2'-bithiophen)-5-ylethynyl)-2-(3,5-bis(trifluoromethyl)phenyl)-2H-benzo[d][1,2,3]triazole (**1g**):* From 5-ethynyl-2,2'-bithiophene (**4g**) (0.076 g, 0.40 mmol), derivative **1g** (0.100 g, 71%) was obtained as a deep-red solid by chromatography eluting with hexane/ethyl acetate (9/1). M. p.: 177–179 °C. ^{1}H-NMR ($CDCl_3$, ppm) δ: 8.99 (s, 2H, *o*-N-Ph), 8.00 (s, 1H, *p*-N-Ph), 7.64 (s, 2H, H-benzotriazole), 7.38 (d, *J* = 3.4 Hz, 2H, H5-thiophene), 7.24–7.29 (m, 4H, H1,2-thiophene), 7.14 (d, *J* = 3.4 Hz, 2H, H3-thiophene), 7.06 (t, *J* = 3.4 Hz, 2H, H4-thiophene). ^{13}C-NMR ($CDCl_3$, ppm) δ: 145.1, 140.8, 140.3, 136.5, 134.1, 133.4, 131.4, 128.0, 125.4, 124.6, 123.7, 121.0, 120.9, 114.0, 110.3, 110.0, 90.9, 89.7. MS calcd for ($C_{34}H_{15}F_6N_3S_4$) $M^{+\cdot}$ 707.0048, found 707.0042.

*4.2.5. 4,7-bis(benzo[b]thiophen-2-ylethynyl)-2-(3,5-bis(trifluoromethyl)phenyl)-2H-benzo[d][1,2,3]triazole (**1h**):* From 2-ethynylbenzo[*b*]thiophene (**4h**) (0.064 g, 0.40 mmol),

derivative **1h** (0.122 g, 94%) was obtained as an orange solid by chromatography eluting with hexane/ethyl acetate (9/1). M. p.: 273–274 °C. ^{1}H-NMR ($CDCl_3$, ppm) δ: 9.18 (s, 2H, *o*-N-Ph), 8.14 (s, 1H, *p*-N-Ph), 7.81–7.86 (m, 4H, *o*-H-benzothiophene), 7.73 (s, 2H, H-benzotriazole), 7.72 (s, 2H, H-thiophene), 7.39–7.42 (m, 4H, *m*-H-benzothiophene). ^{13}C-NMR ($CDCl_3$, ppm) δ: 145.2, 140.8, 131.9, 130.1, 125.9, 125.8, 124.9, 124.2, 122.3, 122.0, 121.0, 114.2, 91.1, 90.2, 82.5. MS calcd for ($C_{34}H_{15}F_6N_3S_2$) $M^{+\cdot}$ 643.0606, found 643.0621.

*4.2.6. 4,7-bis(benzo[b]thiophen-7-ylethynyl)-2-(3,5-bis(trifluoromethyl)phenyl)-2H-benzo[d][1,2,3]triazole (**1i**):* From 7-ethynylbenzo[*b*]thiophene (**4i**) (0.064 g, 0.40 mmol), derivative **1i** (0.101 g, 77%) was obtained as a yellow solid by chromatography eluting with hexane/ethyl acetate (9/1). M. p.: 180–182 °C. ^{1}H-NMR ($CDCl_3$, ppm) δ: 9.16 (s, 2H, *o*-N-Ph), 8.01 (s, 1H, *p*-N-Ph), 7.89 (d, *J* = 7.4 Hz, 2H, *p*-H-benzothiophene), 7.75 (s, 2H, H-benzotriazole), 7.70 (d, *J* = 7.4 Hz, 2H, *o*-H-benzothiophene), 7.59 (d, *J* = 5.4 Hz, 2H, H2-thiophene), 7.45 (t, *J* = 7.4 Hz, 2H, *m*-H-benzothiophene), 7.44 (d, *J* = 5.4 Hz, 2H, H3-thiophene). ^{13}C-NMR ($CDCl_3$, ppm) δ: 145.6, 142.9, 140.9, 139.6, 133.4, 131.2, 127.8, 127.2, 124.6, 124.4, 124.3, 123.9, 120.9, 117.1, 114.4, 95.4, 89.3. MS calcd for ($C_{34}H_{15}F_6N_3S_2$) $M^{+\cdot}$ 643.0606, found 643.0625.

4.2.7. 4,*4'-((2-(3,5-bis(trifluoromethyl)phenyl)-2H-benzo[d][1,2,3]triazole-4,7-diyl)bis(ethyne-2,1-diyl))dianiline (**1j**)*: From 4-ethynylaniline (**4j**) (0.047 g, 0.40 mmol), derivative **1j** (0.050 g, 45%) was obtained as an orange solid by chromatography eluting with hexane/ethyl acetate (9/1). M. p.: 166–168 °C. ^{1}H-NMR ($CDCl_3$, ppm) δ: 8.92 (s, 2H, *o*-N-Ph), 8.02 (s, 1H, *p*-N-Ph), 7.55 (s, 2H, H-benzotriazole), 7.29 (d, *J* = 7.8Hz, 4H, *o*-Ph), 6.59 (d, *J* = 7.8 Hz, 4H, *m*-Ph), 3.80 (s, 4H, NH_2). ^{13}C-NMR ($CDCl_3$, ppm) δ: 146.9, 144.8, 140.6, 133.4, 131.4, 130.7, 123.1, 121.1, 114.5, 113.7, 111.3, 110.5, 84.3. MS calcd for ($C_{30}H_{17}F_6N_5$) $M^{+\cdot}$ 561.1383, found 561.1371.

*4.2.8. 4,4'-((2-(3,5-bis(trifluoromethyl)phenyl)-2H-benzo[d][1,2,3]triazole-4,7-diyl)bis(ethyne-2,1-diyl))bis(N,N-diphenylaniline) (**1k**):* From 4-ethynyl-*N,N*-diphenylaniline (**4k**) (0.108 g, 0.40

mmol), derivative **1k** (0.150 g, 87%) was obtained as an orange solid by chromatography, eluting with hexane/ethyl acetate (99/1). M. p.: 168–170 °C. ^{1}H-NMR ($CDCl_3$, ppm) δ: 8.98 (s, 2H, *o*-N-Ph), 7.98 (s, 1H, *p*-N-Ph), 7.61 (s, 2H, H-benzotriazole), 7.52 (d, *J* = 9.2 Hz, 4H, *o*-Ph), 7.05–7.32 (m, 24H, H-arom). ^{13}C-NMR ($CDCl_3$, ppm) δ: 148.6, 147.0, 145.5, 140.9, 133.3, 133.0, 132.9, 131.4, 129.5, 125.3, 123.9, 121.8, 121.0, 115.0, 114.3, 97.9, 84.3. MS calcd for ($C_{54}H_{33}F_6N_5$) $M^{+\cdot}$ 865.2635, found 865.2643.

*4.2.9. 9,9'-(((2-(3,5-bis(trifluoromethyl)phenyl)-2H-benzo[d][1,2,3]triazole-4,7-diyl)bis(ethyne-2,1-diyl))bis(4,1-phenylene))bis(9H-carbazole) (**1l**)*: From 1-ethynylpyrene (**4l**) (0.107 g, 0.40 mmol), derivative **1l** (0.122 g, 71%) was obtained as a pale orange solid by chromatography eluting with hexane/ethyl acetate (9/1). M. p.: 308–310 °C. ^{1}H-NMR ($CDCl_3$, ppm) δ: 9.04 (s, 2H, *o*-N-Ph), 8.17 (d, *J* = 7.8 Hz, 4H, H4-carbazole), 8.02 (s, 1H, *p*-N-Ph), 7.95 (d, *J* = 7.8 Hz, 4H, H1-carbazole), 7.75 (s, 2H, H-benzotriazole), 7.68 (d, *J* = 8.3 Hz, 4H, *o*-Ph), 7.49 (d, *J* = 8.3 Hz, 4H, *m*-Ph), 7.45 (t, *J* = 7.8 Hz, 4H, H2-carbazole), 7.32 (t, *J* = 7.8 Hz, 4H, H3-carbazole). ^{13}C-NMR ($CDCl_3$, ppm) δ: 145.6, 140.5, 138.4, 133.5, 133.3, 132.0, 130.8, 128.8, 126.9, 126.1, 123.7, 123.3, 121.4, 120.4,120.3, 114.4, 110.0, 109.7, 96.7, 85.6. MS calcd for ($C_{54}H_{29}F_6N_5$) $M^{+\cdot}$ 861.2322, found 861.2345.

*4.2.10. 10,10'-(((2-(3,5-bis(trifluoromethyl)phenyl)-2H-benzo[d][1,2,3]triazole-4,7-diyl)bis(ethyne-2,1-diyl))bis(4,1-phenylene))bis(10H-phenoxazine) (**1m**):* From 10-(4-ethynylphenyl)-10*H*-phenoxazine (**4m**) (0.082 g, 0.40 mmol), derivative **1m** (0.140 g, 79%) was obtained as a red solid by chromatography eluting with hexane/ethyl acetate (9/1). M. p.: 343–344 °C. ^{1}H-NMR ($CDCl_3$, ppm) δ: 9.02 (s, 2H, *o*-N-Ph), 8.02 (s, 1H, *p*-N-Ph), 7.93 (d, *J* = 7.8 Hz, 4H, *o*-Ph), 7.73 (s, 2H, H-benzotriazole), 7.44 (d, J = 7.8 Hz, 4H, *m*-Ph), 6.61–6.73 (m, 12H, H-phenoxazine), 6.00 (d, *J* = 7.9 Hz, 4H, H4-phenoxazine). ^{13}C-NMR ($CDCl_3$, ppm) δ: 145.5, 144.0, 140.9, 139.7, 134.7, 134.0, 133.1, 132.0, 131.2, 123.3, 123.2, 121.7, 121.1, 115.6, 114.4, 113.3, 96.4, 85.9. MS calcd for ($C_{54}H_{29}F_6N_5O_2$) $M^{+\cdot}$ 893.2220, found 893.2260.

Acknowledgements

Financial support from the MINECO of Spain (project CTQ2014-53600-R) and CTQ2014-52331R), UCLM (GI20163531) and Gobierno de Aragón (Research Group E39) is gratefully acknowledged. I. Torres is indebted to MEC for an FPU studentship. Moreover, technical support from the High Performance Computing Service of the University of Castilla-La Mancha is gratefully acknowledged.

References

[1] (a) Duan L, Qiao J, Sun Y, Qiu, Y. Strategies to Design Bipolar Small Molecules for OLEDs: Donor-Acceptor Structure and Non-Donor-Acceptor Structure. Adv Mater 2011;23:1137-1144. doi: 10.1002/adma.201003816. (b) Friend RH., Gymer RW, Holms AB, Burroughes JH, Marks RN, Taliani C, Bradley DDC, Dos Santos DA, Brédas JL, Lögdlund M, Salaneck WR. Electroluminescence in conjugated polymers. Nature 1999;397:121-128 doi:10.1038/16393. (c) Grimsdale AC, Chan KL, Martin RE, Jokisz PG, Holmes AB. Synthesis of Light-Emitting Conjugated Polymers for Applications in Electroluminescent Devices. Chem Rev 2009;109:897-1091. doi:10.1021/cr000013v. (d) Qin T, Wiedermair W, Nau S, Trattnig R, Sax S, Winkler S, Vollmer A, Koch N, Baumgarten M, List EJW, Müllen K. Core, Shell, and Surface-Optimized Dendrimers for Blue Light-Emitting Diodes. J Am Chem Soc 2011;133:1301-1303. doi:10.1021/ja109734e.

[2] (a) Zhou Y, Liu W, Ma Y, Wang H, Qi L, Cao Y, Wang J, Pei J. Single Microwire Transistors of Oligoarenes by Direct Solution Process. J Am Chem Soc 2007;129:12386-12387. doi:10.1021/ja075045f. (b) Briseno, AL, Mannsfeld SCB, Reese C, Hancook, JM, Xiong Y, Jenekhe SA, Bao Z, Xia Y. Perylenediimide Nanowires and Their Use in Fabricating Field-Effect Transistors and Complementary Inverters. Nano Lett 2007;7:2847-2853. doi: 10.1021/nl071495u. (c) Jiang L, Fu Y, Li H, Hu W. Single-Crystalline, Size, and Orientation Controllable Nanowires and Ultralong Microwires of Organic Semiconductor with Strong Photoswitching Property. J Am Chem Soc. 2008;130:3937-3941. doi:10.1021/ja07760. (d) Wang C, Dong H, Hu W, Liu Y, Zhu D. Semiconducting p-Conjugated Systems in Field-Effect Transistors: A Material Odyssey of Organic Electronics. Chem Rev 2012;112:2208-2267. doi:10.1021/cr100380z.

[3] (a) Wang D, Hao C, Zheng W, Peng Q, Wang T, Liao Z, Yu D, Li Y. Ultralong Single-Crystalline Ag2S Nanowires: Promising Candidates for Photoswitches and Room-Temperature Oxygen Sensors. Adv Mater 2008;20:2628-2632. doi: 10.1002/adma.200800138. (b) Che Y, Yang X, Liu G, Yu C, Ji H, Zuo J, Zhao J, Zang L. Ultrathin n-Type Organic Nanoribbons with High Photoconductivity and Application in Optoelectronic Vapor Sensing of Explosives. J Am Chem Soc 2010;132:5743-5750. doi: 10.1021/ja909797q (c) Naddo T, Che YK,

Zhang W, Blakrishnan K, Yang XM, Yen M, Zhao JC, Moore JS, Zang L. Detection of Explosives with a Fluorescent Nanofibril Film. J Am Chem Soc 2007;129:6978-6979. doi:10.1021/ja070747. (d) Che Y, Yang X, Loser S, Zang L. Expedient Vapor Probing of Organic Amines Using Fluorescent Nanofibers Fabricated from an n-Type Organic Semiconductor. Nano Lett 2008;8:2219-2223. doi: 10.1021/nl080761g.

[4] O'Carroll, Lieberwirth I, Redmond G. Microgravity effects and optically pumped lasing in single conjugated polymer nanowires. Nat Nanotechnol 2007;2:180-184. doi:10.1038/nnano.2007.35.

[5] (a) Law M, Surbuly DJ, Johnson JC, Goldberger J, Saykally RJ, Yang P. Nanoribbon Waveguides for Subwavelength Photonics Integration. Science 2004;305:1269-1273. doi: 10.1126/science.1100999. (b) Takazawa K, Kitahama Y, Kimura Y, Kido G. Optical Waveguide Self-Assembled from Organic Dye Molecules in Solution. Nano Lett 2005;5:1293-1296. doi: 10.1021/nl050469y. (c) Gu X, Yao J, Zhang G, Yan Y, Zhang C, Peng Q, Liao Q, Wu Y, Xu Z, Zhao Y, Fu H, Zhang D. Polumorphism-Dependent Emission for Di(p-methoxyphenyl)dibenzofulvene and Abalogurs: Optical Waveguide/Amplified Spontaneous emission Behaviors. Adv Funct Mater 2012;22:4862-4872. doi: 10.1002/adfm.201201482. Alguna mas

[6] (a) Tong L, Gattass RR, Ashcom JB, He SL, Lou JY, Shen MY, Maxwell I, Mazur E. Subwavelength-diameter silica wires for low-loss optical wave guiding. Nature 2003;426:816-819. doi:10.1038/nature02193. (b) Zheng JY, Yang YL, Wang XP, Zhao YS, Huang JX , Yao JN. Wire-on-Wire Growth of Fluorescent Organic Heterojunctions. J Am Chem Soc 2012;134:2880-2883. doi: 10.1021/ja209815f.. (c) Kong Q, Liao Q, Xu Z, Wang X, Yao, Fu H. Epitaxial Self-assembly of Binary Molecular Components into Branched Nanowire Heterostructures for Photonic Applications. J Am Chem Soc 2014;136:2382-2388. doi: 10.1021/ja410069k. (d) Li Q, Jia Y, Dai L, Yang Y, Li J. Controlled Rod Nanostructured Assembly of Diphenylalanine and Their Optical Waveguide Properties. ACS Nano 2015;9:2689-2695. doi: 10.1021/acsnano.5b00623.

[7] Lei T, Pei J. Solution-processed organic nano- and micro-materials: design strategy, growth mechanism and applications. J Mater Chem 2012;22:785-798. doi: 10.1039/c1jm14599a.

[8] (a) Che Y, Yang X, Balakrishnan K, Zuo J, Zang L. Highly Polarized and Self-Waveguided Emission from Single-Crystalline Organic Nanobelts. Chem Mater 2009;21:2930-2934. doi:10.1021/cm9007409. (b) Liu T, Li Y, Yan Y, Li Y, Yu Y, Chen N, Chen S, Liu C, Zhao Y, Liu H. Tuning Growth of Low-Dimensional Organic Nanostructures for Efficient Optical Waveguide Applications. J Phys Chem C 2012;116;14134-14138. doi: 0.1021/jp301998d. (c) Guo ZH, Lei T, Jin ZX, Wang JY, Pei J. Organic lett 2013;15:33530-3533. doi: 10.1021/ol4012025.

[9] Meier H. Conjugated Oligomers with Terminal Donor–Acceptor Substitution. Angew Chem Int Ed 2005;44:2482-2506. doi: 10.1002/anie.200461146.

[10] (a) Mulliken RS, Person WB. Donor-Acceptor Complexes. Annu Rev Phys Chem 1962;13:107-126. doi: 10.1146/annurev.pc.13.100162.000543. (b) Foster R. In Organic Charge-Transfer Complexes. New York: Academic Press; 1969. (c) Foster R. Electron Donor-Acceptor Complexes. J Phys Chem 1980;84:2135-2141.

doi: 10.1021/j100454a006. (d) Wang JL, Xiao Q, Pei J. Benzothiadiazole-Based D-π-A-π-D Organic Dyes with Tunable Band Gap: Synthesis and Photophysical Properties. Org Lett 2010;12:4164-4167. doi: 10.1021/ol101754q. (e) Homnick PJ, Tinkham JS, Devaughn R, Lahti PM. Engineering Frontier Energy Levels in Donor−Acceptor Fluoren-9-ylidene Malononitriles versus Fluorenones. J Phys Chem A 2014;118:475-486. doi: 10.1021/jp407854r (f) Lu X, Fan S, Wu J, Jia X, Wang ZS, Zhou G. Controlling the Charge Transfer in D−A−D Chromophores Based on Pyrazine Derivatives. J Org Chem 2014;79:6480-6489. doi: 10.1021/jo500856k. (g) Turro NJ, Ramamurthy V, Scaianon JC. In Modern Molecular Photochemistry of Organic Molecules, Sausalito, University Science Books, 2010. (h) Turro NJ, Ramamurthy V, Scaiano JC. Modern Molecular Photochemistry of Organic Molecules. Photochem Photobiol 2012;88:1033 .

[11] (a) Qian G, Dai B, Luo M, Yu D, Zhan J, Zhang Z, Ma D, Wang Z Y. Band Gap Tunable, Donor-Acceptor-Donor Charge-Transfer Heteroquinoid-Based Chromophores: Near Infrared Photoluminescence and Electroluminescence. Chem Mat 2008;20:6208-6216. doi: 10.1021/cm801911n. (b) Tao T, Ma BB, Peng YX, Wang XX, Huang W, You XZ. Asymmetrical/Symmetrical D−π−A/D−π−D Thiazole-Containing Aromatic Heterocyclic Fluorescent Compounds Having the Same Triphenylamino Chromophores. J Org Chem 2013:78:8669-8679. doi: 10.1021/jo401384g.

[12] (a) Li Y, Liu T, Liu H, Tian MZ, Li Y. Self-Assembly of Intramolecular Charge-Transfer Compounds into Functional Molecular Systems. Acc Chem Res 2014;47:1186-1198. doi: 10.1021/ar400264e. (b) Li Y, Quing Z, Yu Y, Liu T, Jiang R, Li Y. Synthesis and Self-Assembly of Dihydroxyperylene Bisimides for the Tuning of Photophysical Properties. Chem Asian J 2012;7:1934-1939. doi: 10.1002/asia.201200243.

[13] Patel DG, Feng F, Ohnishi Y, Abboud KA, Hirata S, Schanze KS, Reynolds JR. It Takes More Than an Imine: The Role of the Central Atom on the Electron-Accepting Ability of Benzotriazole and Benzothiadiazole Oligomers. J Am Chem Soc 2012;134:2599-2612. doi: 0.1021/ja207978v.

[14] (a) Wettach H, Pasker F, Höger S. 2-Aryl-2*H*-benzotriazoles as Building Blocks for New Low-Bandgap Poly(arylene-ethynylene)s. Macromolecules 2008;41:9513-9515. doi: 10.1021/ma802127q. (b) Pasker FM, Kein MFG, M. Sanyal M, Barrena E, Lemmer U, Colsmann A, Höger S. Photovoltaic Response to Structural Modifications on a Series of Conjugated Polymers Based on 2-Aryl-2H-benzotriazoles. J Polym Sci Part A Poly Chem 2011;49:5001-5011. doi: 10.1002/pola.24959.

[15] Cáceres D, Cebrián C, Rodríguez AR, Carrillo JR, Díaz-Ortiz A, Prieto P, Aparicio F, García F, Sánchez L. Optical waveguides from 4-aryl-4*H*-1,2,4-triazole-based supramolecular structures. Chem Commun 2013;49:621-623. doi: 10.1039/c2cc37381e.

[16] Pastor MJ, Torres I, Cebrián C, Carrillo JR, Díaz-Ortiz A, Matesanz E, Buendía J, García F, Barberá J, Prieto P Sánchez L. 4-Aryl-3,5-bis(arylethynyl)aryl-4*H*-1,2,4-triazoles: Multitasking Skeleton as a Self-Assembling Unit. Chem Eur J 2015;21:1795-1802. doi: 10.1002/chem.201404243.

[17] Torres I, Carrillo JR, Díaz-Ortiz A, Martín R, Gómez MV, Stegemann L, Strassert CA, Orduna J, Buendía J, Greciano EE, Valera JS, Matesanz E, Sánchez L, Prieto P. Self-assembly of T-shape 2*H*-benzo[d][1,2,3]-triazoles. Optical waveguide and photophysical properties. RSC Adv 2016;6:36544-36553. doi: 10.1039/c6ra02473d.

[18] (a) Roncali J. Synthetic Principles for Bandgap Control in Linear π-Conjugated Systems. Chem Rev 1997;97:173-205. doi: 10.1021/cr950257t. (b) Guo ZH, Lei T, Jin ZX, Wang JY, Pei J. T-Shaped Donor- Acceptor Molecules for Low-Loss Red-Emission Optical Waveguide. Org Lett 2013;15:3530-3533. doi: 10.1021/ol4012025. (c) Lu X, Fan S, Wu J, Jia X, Wang ZS, Zhou G. Controlling the Charge Transfer in D-A-D Chromophores Based on Pyrazine Derivatives. J Org Chem 2014;79:6480-6489. doi: 10.1021/jo500856k.

[19] (a) Varughese S, Non Covalent routes to tune the optical properties of molecular materials. J Mater Chem C 2014;2:3499-3516. doi: 10.1039/C3TC32414A. (b) Wang XA, Zhou Y, Lei T, Hu N, Chen EQ, Pei J. Structural-Property Relationship in Pyrazino[2,3-g]quinoxaline Derivatives: Morphology, and Waveguide Properties. Chem Mater 2010;22:3735-3745. doi: 0.1021/cm100798q.

[20] (a) Koch W Holthausen MC. In A Chemist's Guide to Density Functional Theory. 2nd Ed. Weinheim: Wiley-VCH;2001. ISBN: 978-3-527-30372-4. (b) Cramer CJ. In Essentials of Computational Chemistry: Theories and Models, 2nd ed. Chichester: John Wiley & Sons: 2004. ISBN: 978-0-470-09182-1. (c) Bachrach SM. In Computational Organic Chemistry, 2nd ed. Weinheim: John Wiley & Sons; 2014. ISBN: 978-1-118-29192-4.

[21] (a) Ando S, Murakami R, Nishida JI, Tada H, Inoue Y, Tokito S, Yamashita Y. n-Type Organic Field-Effect Transistors with Very High Electron Mobility Based on Thiazole Oligomers with Trifluoromethylphenyl Groups. J Am Chem Soc 2005;127;14996-14997. doi: 10.1021/ja055686. (b) Deng P, Yan Y. Wang SD, Zhang Q. Naphthoylene(trifluoromethylbenzimidazole) dicarboxylic acid imides for high-performance organic field-effect transistors. Chem Commun 2012;48:2591-2593. doi: 10.1039/C2CC17272K. (c) Sonar P, Ng GM, Lin TT, Dodabalapur A, Chen ZK. Solution processable low bandgap diketopyrrolopyrrole (DPP) based derivatives novel acceptors for organic solar cells. J Mat Chem 2010;20:3626-3636. doi: 10.1039/B924404B.

[22] Chung JW, You Y, Huh HS, An BK, Yoon SJ, Kim SH, Lee SW, Park SY. Shear- and UV-Induced Fluorescence Switching in Stilbenic π-Dimer Crystals Powered by Reversible [2+2] cycloaddition. J Am Chem Soc 2009, 131, 8163-8172. doi: 10.1021/ja900803d.

[23] Andzelm J, Kölmel C, Klamt A. Incorporation of solvent effects into density functional calculations of molecular energies and geometries. J Chem Phys 1995;103:9312-9320 . doi: 10.1063/1.469990.

[24] Adamo C, Jacquemin D. The Calculations of Excited-State Properties with Time-Dependent Density Functional Theory. Chem Soc Rev 2013;42:845-856. doi: 10.1039/C2CS35394F.

[25] (a) DG. Zhao Y, Truhlar D G. The M06 suite of density functionals for main group thermochemistry, thermochemical kinetics, noncovalent interactions, excited states, and transition elements: two new functionals

and systematic testing of four M06-class functionals and 12 other functionals. Theor Chem Acc 2008;120:215-241. doi: 10.1007/s00214-007-0310-x.

[26] (a) Martínez de Baroja N, Franco S, Garín J, Orduna J, Villacampa B, Borja P, Alicante R. Synthesis, Characterization, and optical properties of novel 1,3-dithiole donor-based chromophores. RSC Adv 2013;3:2953-2962. doi: 10.1039/C2RA23235A. (b) (a) Li R, Zheng J, Truhlar D. G. The M06 suite of density functionals for main group thermochemistry, thermochemical kinetics, noncovalent interactions, excited states, and transition elements: two new functionals and systematic testing of four M06-class functionals and 12 other functionals. Theor. Chem. Acc., 2008:120:215-241. doi: 10.1007/s00214-007-0310-x.

[27] (a) Yang B, Kim SK, Xu H, Park Y, Zhang H, Gu C, Shen F, Wang C, Liu D, Liu X, Hanif M, Tang S, Li W, Li F, Shen J, Park JW, Ma Y. The Origin of the Improved Efficiency and Stability of Triphenylamine-Substituted Anthracene Derivatives for OLEDs: A Theoretical Investigation. ChemPlusChem 2008;9:2601-2609. doi: 10.1002/cphc.200800513. (b) W. Li, D. Liu, F. Shen, D. Ma, Z. Wang, T. Feng, Y. Xu, B. Yang, Y. Ma. A Twisting Donor-Acceptor Molecule with an Intercrossed Excited State for Highly Efficient, Deep-Blue Electroluminescence. Adv Funt Mater 2012;22:2797-2803. doi: 10.1002/adfm.201200116.

[28] Chou HH, Chen YC, Huang HJ, Lee TH, Lin JT, Tsai C, Chen K. High-performance dye-sensitized solar cells based on 5,6-bis-hexyloxy-benzo[2,1,3]thiadiazole. J Mater Chem 2012;22:10929-10938. doi: 10.1039/C2JM30427A.

[29] Clarke TM, Gordon KC, Kwok WM, Philips DL, Officer DL. Tuning from ∂,∂^* to Charge-Transfer Excited States in Styryl-Substituted Terthiophenes: An Ultrafast and Steady-State Emission Study. J Phys Chem A 2006;110:7696-7702. doi: 10.1021/jp0600312.

[30] (a) Tong M, Gattass RR, Ashcom JB, He S, Lou J, Shen M, Maxwell I, Mazur E. Subwavelength-diameter silica wires for low-loss optical wave guiding. Nature 2003;426:816-819. doi: 10.1038/nature02193. (b) Zhao YS, Peng AD, Fu H, Ma Y, Yao J. Nanowire Waveguides and Ultraviolet Lasers Based on Small Organic Molecules. Adv Mater 2008;20:16611665. doi: 10.1002/adma.200800123. (c) Figueira-Duarte TM, Müller K. Pyrene-Based Materials for Organic Electronics. Chem Rev 2011;111:7260-7314. doi.10.1021/cr100428a.

[31] Takazawa K, Kitahama Y, Kimura Y and Kido G. Optical Waveguide Self-Assembled from Organic Dye Molecules in Solution. Nano Lett 2005;5:12931296. doi: 10.1021/nl050469y.

[32] Frisch MJ, Trucks GW, Schlegel HB, Scuseria GE, Robb MA, Cheeseman JR, Scalmani G, Barone V, Mennucci B, Petersson GA, Nakatsuji H, Caricato M, Li X, Hratchian HP, Izmaylov FA, Bloino J, Zheng G, J. Sonnenberg JL, Hada M, Ehara M, Toyota K, Fukuda R, Hasegawa J, Ishida M, Nakajima T, Honda Y, Kitao O, Nakai H, Vreven T,Montgomery JA Jr, Peralta JE, Ogliaro F, Bearpark M, Heyd JJ, Brothers E, Kudin KN, Staroverov VN, Kobayashi R, Normand J, Raghavachari K, Rendell A, Burant JC, Iyengar SS, Tomasi SJ, Cossi M, Rega N, Millam NJ, Klene M, Knox JE, Cross JB, Bakken V, Adamo C, Jaramillo J, Gomperts R, Stratmann RE, Yazyev O, Austin AJ, Cammi R, Pomelli C, Ochterski JW, Martin RL, Morokuma K, Zakrzewski VG, Voth GA,

Salvador P, Dannenberg JJ, Dapprich S, Daniels AD, Farkas O, Foresman JB, Ortiz JV, Cioslowski J, Fox DJ. Gaussian 09, Revision A.1, Gaussian, Inc., Wallingford CT, 2009.

[33] (a) McLean AD, Chandler GS, "Contracted Gaussian-basis sets for molecular calculations. 1. 2nd row atoms, Z=11-18," J. Chem. Phys. 1980:72:5639-48. doi:10.1063/1.438980 (b) .Raghavachari K, Binkley JS, Seeger R, Pople JA, "Self-Consistent Molecular Orbital Methods. 20. Basis set for correlated wave-functions," J. Chem. Phys., 1980:72:650-54. doi:10.1063/1.438955.

[34] (a) Klamt A, Schürmann G J. COSMO: a new approach to dielectric screening in solvents with explicit expressions for the screening energy and its gradients. Chem Soc Perkin Trans 2;1993:799-805. doi: 10.1039/P29930000799. (b) Andzelm J, Kölmel C, Klamt A. Incorporation of solvent effects into density functional calculations of molecular energies and geometries. J Chem Phys 1995;103:9312-9320. doi: 10.1063/1.469990 (c) Barone V, Cossi M. Quantum Calculation of Molecular Energies and Energy Gradients in Solution by a Conductor Solvent Model. J Phys Chem A 1998;102:1995-2001. doi: 10.1021/jp9716997. (d) Cossi M, Rega N, Scalmani G, Barone V. Energies, Structures, and Electronic Properties of Molecules in Solution with the C-PCM Solvation Model. J Comput Chem 2003;24:669-681. doi: 10.1002/jcc.10189.